The cross-sectional resistance of square and rectangular hollow steel sections loaded by bending moment and shear force

The cross-sectional resistance of square and rectangular hollow steel sections loaded by bending moment and shear force

Thomas Haan, Davide Leonetti [*], Herm Hofmeyer, H.H (Bert) Snijder

Eindhoven University of Technology, Eindhoven, The Netherlands

ARTICLE INFO

ABSTRACT

This paper presents an evaluation of the design rules for the bending moment–shear force ($M - V$) interaction of cold- and hot-formed square, and rectangular hollow steel sections (SHS & RHS). More specifically, the design rules, as provided by EN1993-1-1 regarding RHS and SHS of section class 1 and 2 are covered for the steel grades S235 up to and including S460. A 4-point bending test was simulated by means of a finite element model, which was validated on the basis of experimental tests from existing literature. A parametric study was performed and numerical $M - V$ interaction results were compared to the provisions in EN1993-1-1. This comparison indicates that the current design rules in EN1993-1-1 regarding $M - V$ interaction are conservative and overestimate the reduction of the bending resistance due to the presence of shear. Alternative design rules for the shear area and $M - V$ interaction of RHS and SHS are proposed and evaluated by means of a statistical assessment procedure based on existing literature and EN1990-1-1. Both newly developed design rules are shown to ensure an adequate reliability level when a partial safety factor equal to 1 is used.

1. Introduction

Structural steel is a widely applied building material within the built environment, mainly due to its isotropic material behavior and relatively high stiffness and strength as compared to alternative structural building materials. For the design of steel structures within the European Union, 'EN1993-1-1: Design of steel structures' [1] prescribes a set of design rules to guarantee a predetermined structural safety level. In the case of solely bending moment M applied, the resistance of a steel section is predicted well. However, if a section is subjected to a bending moment and a shear force V, the prediction of the cross-sectional resistance is less straightforward. This is due to an effect of the applied shear force on the bending moment resistance, also known as $M - V$ interaction.

The current design rule for $M - V$ interaction in EN1993-1-1 is based in part on the research of Drucker [2], who developed a design rule based on the assumption that the web of an I-shaped section without root radii resists the shear force and the flanges resist the bending moment. When a combination of a bending moment around the strong axis of a section and its associated shear force is applied, EN1993-1-1 [1] also assumes that the web(s) of the section primarily resist the shear force and the flanges mainly resist the bending moment. For RHS and SHS this results in the stress distribution shown in Fig. 1.

For relatively low shear force, the bending resistance will not be significantly influenced. However, with increasing shear force, the

bending resistance of the section reduces significantly. To calculate the $M - V$ resistance of a section according to EN1993-1-1 [1], the plastic shear resistance $V_{pl,Rd}$ should be calculated [1]:

$$V_{pl,Rd} = \frac{A_v * f_y}{\sqrt{3}}, \tag{1}$$

where A_v is the shear area of the section, calculated according to:

$$(a) \quad A_v = \frac{A * h}{b + h}, \qquad (b) \quad A_v = \frac{A * b}{b + h}, \tag{2}$$

with Eq. (2)(a) for strong-axis, and (2)(b) for weak-axis bending. In this equation, A is the area of the cross-section, h its height, and b its width.

If the shear utilization ratio n, that is, the ratio between the acting shear force V_{Ed} and the plastic shear resistance, exceeds 0.5, the plastic bending resistance $M_{pl,Rd}$ shall should be calculated with a reduced yield strength for the shear area. EN1993-1-1 [1] gives an equation for the reduction of the yield strength for the shear area $f_{y,r,T}$ based on the Tresca yield criterion:

$$f_{y,r,T} = (1 - \rho) * f_y, \tag{3}$$

where $1 - \rho$ is a reduction factor for the yield stress. ρ Is calculated according to:

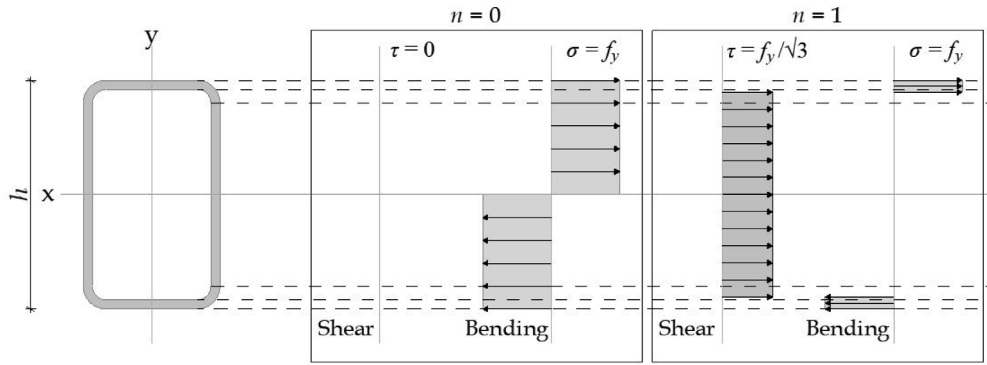$$\rho = (2n - 1)^2 \qquad (\text{for} \quad n > 0.5). \tag{4}$$

Fig. 1. Theoretical plastic bending and shear stresses visualized for shear utilization ratios of $n = 0$ and $n = 1$.
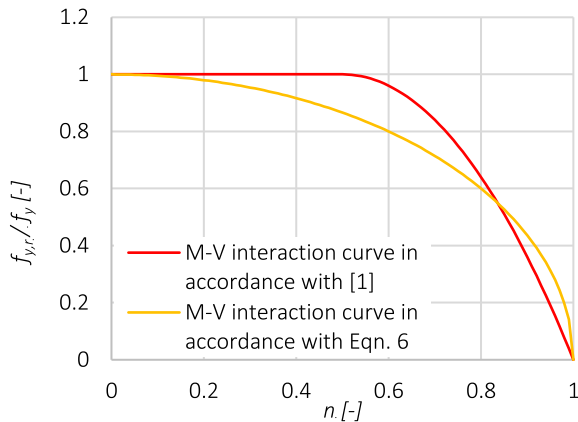

Fig. 2. Relative reduced shear yield stress against an increasing shear utilization ratio, based on the Tresca and Von Mises yield criterion.

Eq. (3) is plotted in Fig. 2 where, on the x-axis, the shear utilization ratio n, and on the y-axis, $f_{y,r,T}$ are shown.

With this information, and in line with the design rule for I-shaped cross-sections in EN1993-1-1 [1], it is assumed that the reduced bending resistance $M_{v,Rd}$ is calculated according to:

$$(a) \quad M_{y,v,Rd} = M_{pl,y} - W_{pl,y,v} * (f_y - f_{y,r,T}),$$
$$(b) \quad M_{z,v,Rd} = M_{pl,z} - W_{pl,z,v} * (f_y - f_{y,r,T}), \tag{5}$$

with Eq. (5)(a) for strong,- and (5)(b) for weak-axis bending. In this equation, $W_{pl,v}$ is the plastic section modulus of the shear area.

The design rules on $M - V$ interaction were developed over the last century. Research on sections, subjected to solely shear force, was already conducted in 1855 by Dmitrii Ivanovich Zhuravskii, as reported in [3]. Nevertheless, large-scale research on $M - V$ interaction started around the 1950's, in which reduction of the bending resistance was determined due to the presence of shear force. In 1951, Horne [4] attempted to develop a lower-bound solution for $M - V$ interaction in I-shaped sections, based on a theoretical plane stress slip-line field solution, using a plastic approach based on the Tresca yield criterion. In 1954, Heyman and Dutton [5] conducted similar research in combination with the Von Mises yield criterion. In the same year, Green [6] developed theoretical solutions for the $M - V$ interaction of cantilever beams, and two years later, in 1956, Drucker [2] developed an upper bound solution for $M - V$ resistance in a rectangular section, on which the current design rules in EN1993-1-1 [1] are partly based. Thereafter, Neal [7] considered an axial force N in addition to Drucker's work and obtained a $M - V - N$ interaction relationship in 1961. Furthermore, he derived a lower bound solution for I-shaped sections [8].

More recently, in 2019, Dekker [9] performed research with a primary focus on the $M - V$ interaction of rolled I-shaped steel sections.

This research was carried out as part of the Safebrictile project [10], the primary objective of which was to evaluate the structural safety of structural steel members. Therefore, Safebrictile developed "An objective and consistent safety assessment procedure for the various failure modes that are relevant for steel structures" [10]. Furthermore, within the Safebrictile project, an experimental test program for steel properties was carried out, along with a full-scale $M - V$ interaction test program. Lastly, several design rules in EN1993-1-1 [1] were assessed according to the developed safety assessment procedure [10]. It was concluded that the currently prescribed shear area is too optimistic for the shear resistance of I-shaped sections. Furthermore, the $M - V$ interaction curve predicts a reduction in bending resistance due to the presence of shear at too low values of n. Lastly, this curve shows a too-gradual reduction of the bending resistance for high amounts of shear force. For these three reasons, a set of new design rules for the resistance of rolled I-shaped steel sections, loaded in bending (in the strong axis) and shear, was defined and shown to be adequate [9].

In addition to the results of [9], a second motivational factor for this research is the presence of inconsistency within EN1993-1-1 [1] with respect to the yield criteria [9]. EN1993-1-1 [1] generally makes use of the Von Mises yield criterion. Nevertheless, when it comes to the design rules for $M - V$ resistance of structural steel members (in clause 6.2.8), EN1993-1-1 [1] makes use of the Tresca yield criterion. An approach to the reduction of the yield stress could be described by means of the Von Mises yield criterion ($f_{y,r,VM}$):

$$f_{y,r,VM} = \sqrt{1 - n^2} * f_y. \tag{6}$$

which results in a different theoretical interaction curve, as shown in Fig. 2.

Limited research is dedicated to the cross-sectional resistance of RHS and SHS loaded by bending moment and shear force. In 1999, Wilkinson [11] performed experimental and numerical research on the moment–rotation capacity of cold-formed RHS. In [11], 4-point bending tests are reported on several cold- and hot-formed RHS with the main goal to establish the section classification and slenderness limits for cold-formed RHS [11]. In 2010, Gardner et al. [12] performed comparative experimental research on cold- and hot-formed sections, in which three- and five-point bending tests were performed on cold- and hot-formed sections. The main goal was to assess the influence of the different production routes on the structural responses of the section [12]. In 2016, Wang et al. [13] performed experimental and numerical research on high-strength steel RHS and SHS. In this study, three- and four-point bending tests were performed on hot-formed RHS and SHS, with the main goal to assess the section classification [13]. These three studies have in common that the main goal was to examine the rotation capacity of RHS. Therefore, all tests were performed with relatively low shear utilization ratios. Hence, the behavior of RHS and SHS under bending moments at high shear utilization ratios is still unknown.

The current design rules in EN1993-1-1 [1], regarding the cross-sectional resistance, assume a two-dimensional stress distribution. However, in practice, a complex three-dimensional stress state occurs. Furthermore, due to innovations within the building industry, such as the development of higher-strength steel grades, the design rules in EN1993-1-1 [1] need to be evaluated to ensure an accurate pre-determined safety level. Earlier conducted research regarding $M - V$ interaction suggests that the current design rules of EN1993-1-1 are not accurate [9]. Therefore, this paper presents a numerical and statistical evaluation of the current design rules in EN1993-1-1 [1] regarding the shear and $M - V$ resistance of RHS and SHS, and provides and assesses newly proposed design rules. Section 2 provides the method for the development and assessment of new design rules and Section 3 describes the finite element (FE) model that is developed to execute a parametric study. Section 4 provides the results of this parametric study and the assessment of the existing and newly developed design rules, followed by a discussion of the results in Section 5 and the conclusions of this research in Section 6.

2. Development and assessment of new design rules

The development of the new design rules was carried out in two parts, the development of (1) a corrected version of the current design rule for the shear resistance, and (2) a new design rule for the $M - V$ interaction of RHS and SHS. Thereafter, the newly developed design rules were evaluated by means of the statistical assessment procedure that was developed as a part of the Safebrictile project [10,14,15], which is based on a semi-probabilistic approach, described in Annex D of EN1990 [16].

2.1. Development of a corrected version of the current design rule for the shear resistance

EN1993-1-1 [1] prescribes a design rule to calculate the plastic shear resistance of RHS and SHS (Eq. (1)), in which the shear area is partly based on the h/b ratio of the section and Drucker's equation [2]. The relative shear area A_v/A, can be expressed as a function of the ratio h/b:

$$\frac{A_v}{A} = \frac{h}{h + b} = \frac{h/b}{h/b + 1}. \tag{7}$$

To correct this design rule from possible deviations from experimental data, the correction factor α is introduced in the denominator of Eq. (7). This correction factor is implemented in the denominator of the design rule to ensure a larger correction for larger relative shear areas. The introduction of a correction factor in the numerator of Eq. (7) was also considered, which results in a linear correction of the relative shear area. The second option was disregarded since the resulting design rule proved less accurate. Hence, the resulting equation with an implemented imperfection factor can be described as:

$$\frac{A_v}{A} = \frac{h/b}{\alpha * h/b + 1} \tag{8}$$

Fig. 3 shows a plot of Eq. (8) for different values of α, where the x-axis shows the h/b ratio and the y-axis A_v/A.

Eq. (8) can be rewritten to a design rule for the new shear area $A_{v,new}$:

$$(a) \quad A_{v,new} = \frac{A * h}{\alpha h + b}, \qquad (b) \quad A_{v,new} = \frac{A * b}{\alpha b + h}, \tag{9}$$

with Eq. (9)(a) for strong-axis, and (9)(b) for weak-axis bending. To determine the optimal value of α, a least square estimation was performed [17], in which α was solved for the least square residuals of the resulting shear area from the FE analysis of a section $A_{V,FEA}$, for all tested sections. The summation of the residuals squared S_{res} was calculated in accordance to:

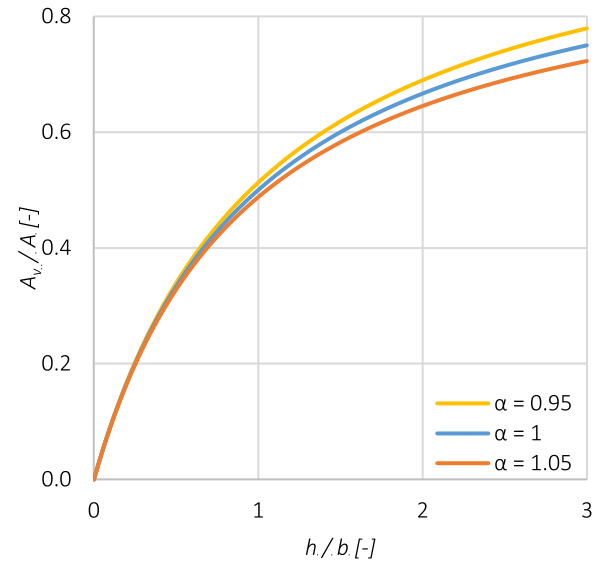$$S_{res} = \sum_{i=1}^{n} (A_{v,FEA,i} - A_{v,new,i})^2. \tag{10}$$

Fig. 3. Relative shear area A_v/A plotted against the height over width ratio of a RHS or SHS for different values of α (0.95, 1, and 1.05).

The corresponding coefficient of determination, R^2, was also calculated, which indicates the percentage of data points that can be predicted by the fitted curve [18]:

$$R^2 = 1 - \frac{S_{res}}{S_{tot}}, \tag{11}$$

where S_{tot} is the squared residual from the mean, calculated according to:

$$S_{tot} = \sum_{i=1}^{n} (A_{v,FEA,i} - \frac{1}{n} \sum_{i=1}^{n} (A_{v,FEA,i}))^2. \tag{12}$$

By theory, the application of the optimal value of α gives a better prediction of the numerical shear area, and thus, a better prediction of the shear resistance [19]. Where the new shear resistance $V_{pl,Rd,new}$ is calculated in accordance with:

$$V_{pl,Rd,new} = \frac{A_{v,new} * f_y}{\sqrt{3}}. \tag{13}$$

The optimal value of the correction factor α is evaluated in Section 4.3 of this paper.

2.2. Development of new design rules for $M - V$ interaction

Similarly, a new design rule was developed for the $M - V$ resistance of RHS and SHS. The $M - V$ interaction design rule, provided by EN1993-1-1 [1], is based on the Tresca yield criterion. According to this design rule, the bending resistance should be reduced if the shear utilization ratio exceeds 0.5. Nevertheless, in general, EN1993-1-1 [1] makes use of the Von Mises yield criterion. Using the Tresca yield criterion for $M - V$ interaction creates an inconsistency. Therefore, an alternative design rule was developed, based on Eq. (6). This equation prescribes a uniform reduction of the yield strength over the total shear area. Nevertheless, the maximum shear stresses are located in the middle parts of the shear area and gradually extend to the outer fibers of the section with an increase in the shear utilization ratio. Therefore, the reduction may be overestimated for low and moderate shear utilization ratios, since the outer fibers of the shear area have a greater impact on the bending resistance, due to a larger lever arm. Furthermore, this equation is based on a 2D beam theory [20], where in reality, a complex 3D stress state occurs. Marginal direct stresses may still arise in the shear of the section due to this stress state.
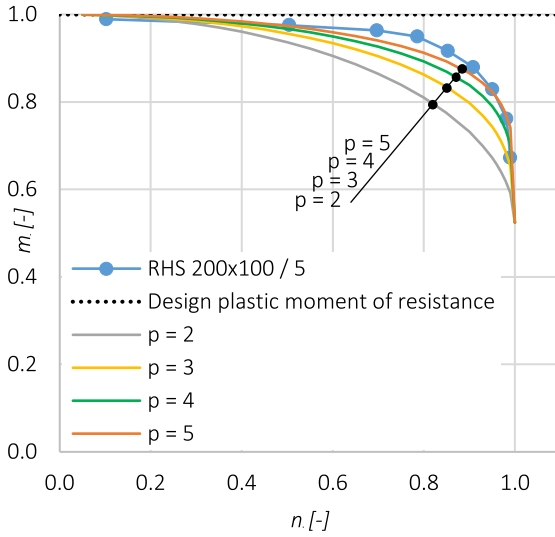
Fig. 4. Comparison of the numerical results of the $M-V$ interaction curve and the theoretical $M-V$ interaction plotted for different values of P, for a RHS 200*100/5 loaded around strong-axis (SA) bending.

To achieve an accurate prediction of the numerical $M-V$ resistance, Eq. (6) should be compensated for (1) the uniform reduction of the yield strength for the total shear area, and (2) marginal direct stresses that may arise within the shear area. The equation, for a reduced yield strength, is based on a root function. Therefore, the reduction can be limited by the application of a higher order root Eq. (6) was rewritten as:

$$f_{y,r,new} = \sqrt[p]{1 - n^2} * f_y, \tag{14}$$

where P is the order of the root. The $M-V$ interaction design rule can then be written as:

$$
\begin{aligned}
(a) \quad & M_{y,v,pl,new} = M_{pl,y} - W_{y,pl,v} * (f_y - f_{y,r,new}), \\
(b) \quad & M_{z,v,pl,new} = M_{pl,z} - W_{z,pl,v} * (f_y - f_{y,r,new}),
\end{aligned} \tag{15}
$$

with Eq. (15)(a) for strong-axis, and (15)(b) for weak-axis bending. In this Equation, $M_{v,pl,new}$ is the bending resistance of a section based on the new design rule (Eq. (14)). With this equation, The bending moment utilization ratio m can be calculated according to:

$$(a) \quad m_y = \frac{M_{y,v,pl,new}}{M_{pl,y}}, \quad (b) \quad m_z = \frac{M_{z,v,pl,new}}{M_{pl,z}}, \tag{16}$$

with Eq. (16)(a) for strong-axis, and (16)(b) for weak-axis bending. To give an indication of the effect of different values of p, the $M-V$ interaction curve was plotted for an RHS 200*100/5 with $p = 2, 3, 4$, and 5 (Fig. 4).

To find the optimal value of p, a least square estimation could be performed [17]. All included sections in the parametric study were taken into account for this estimation, each with a number of data points (varying from $N = 6$ up to and including $N = 10$). The summation of the residuals squared S_{res} was calculated according to:

$$S_{res} = \sum_{i=1}^{n} (m_{FEA,i} - m_{Design,i})^2, \tag{17}$$

where m_{FEA} is the non-dimensional bending moment utilization ratio, calculated by means of the resulting maximum bending moments of the tested sections in the parametric study relative to the theoretical plastic bending moments of these sections. m_{Design} is the same non-dimensional bending moment utilization ratio as a result of the design rule. The optimal value of p is evaluated in Section 4.4 of this paper.

2.3. Statistical evaluation of new design rules for shear and $M-V$ resistance

During the design phase of a structure, nominal values of the geometry are used to calculate the resistance of structural members. However, in practice, material and geometrical imperfections are present. To consider these imperfections, a statistical evaluation method, which incorporates the mean values and standard deviation of the yield strength and cross-sectional dimensions of structural members, can be applied. This statistical assessment procedure [14,15] was developed as a part of the Safebrictile project [10] and is based on Annex D of EN1990-1-1 [16]. It concerns a consistent safety assessment procedure for various failure modes, including the $M-V$ interaction resistance. During the development of this procedure, the semi-probabilistic approach, described in EN1990-1-1 [16], was maintained. To apply this statistical assessment procedure [14,15], five steps should be performed to establish the required parameters:

1. The mean value of the correction factor b_r should be calculated by means of a least square estimation:

$$b_r = \frac{\sum_{i=1}^{N} (r_{exp,i} * r_{t,i})}{\sum_{i=1}^{N} r_{t,i}^2}. \tag{18}$$

In this equation, $r_{exp,i}$ is the numerical (or experimental), and $r_{t,i}$ is the theoretical resistance value for specimen i.

2. The error term δ_i should be calculated in accordance with:

$$\delta_i = \frac{r_{exp,i}}{b_r * r_{t,i}}. \tag{19}$$

The quality of the resistance function can be indicated with the coefficient of variation of the error term V_δ. With the error term, V_δ can be calculated according to:

$$\Delta_i = \ln(\delta_i), \tag{20}$$

$$s_\Delta^2 = \frac{1}{n-1} * \sum_{i=1}^{N} (\Delta_i - \overline{\Delta})^2, \tag{21}$$

$$V_\delta = \sqrt{\exp(s_\Delta^2) - 1}, \tag{22}$$

where $\overline{\Delta}$ is the mean value of all Δ_i, calculated according to:

$$\overline{\Delta} = \frac{1}{N} \sum_{i=1}^{N} \Delta_i. \tag{23}$$

3. The coefficient of variation of the basic input variables $V_{r,t,i}$, such as the steel grade and section dimensions are calculated for every sample with the statistical distributions given in Table 1 and according to:

$$V_{r,t,i}^2 = \frac{1}{r_{t,i}(X_m)^2} * \sum_{j=1}^{k} \left(\frac{\partial r_{t,i}(X_j)}{\partial X_j} * \sigma_j \right)^2. \tag{24}$$

In this equation, $r_{t,i}(X_m)$ is the theoretical resistance based on the mean values for specimen i. Variable X_j refers to the different basic input variables ($X = h, b, t, f_y$), each with a standard deviation σ_j, which can be calculated by multiplying the mean value by the coefficient of variation (c.o.v.). These values are given in Table 1. Often, it is complicated to derive the partial derivatives of the resistance function analytically. Therefore, alternatively, a numerical estimation suffices:

$$\frac{\partial r_{t,i}}{\partial X_j} \approx \frac{r_{t,i}(X_1, .., X_j + \Delta X_j, .., X_k) - r_{t,i}(X_1, .., X_j, .., X_k)}{\Delta X_j}, \tag{25}$$

where ΔX_j is a sufficiently small increment of variable X_j.

Table 1
Mean/nominal values of the input parameter of RHS and SHS, including their coefficient of variation [21].

Parameters	S235	S355	S460			
	f_y	f_y	f_y	b	h	t
Mean/nominal	1.25	1.2	1.15	1	1	0.99
c.o.v. [%]	5.5	5	4.5	0.9	0.9	2.5

Table 2
Values of k_d depending on the number of available test specimens N and if $V_{r,t}$ is known, according to EN 1990-Annex D [16].

N	6	8	10	20	30	∞
$V_{r,t}$ known	3.33	3.27	3.23	3.16	3.13	3.04
$V_{r,t}$ unknown	6.36	5.07	4.51	3.64	3.44	3.04

4. The design value for the resistance function $r_{d,i}$ is calculated and the partial safety factor γ_m^* can be determined. Firstly, the log normal coefficients ($Q_{r,t,i}, Q_\delta$, and Q_i) should be calculated:

$$Q_{r,t,i} = \sqrt{\ln(V_{r,t,i}^2 + 1)}, \tag{26}$$

$$Q_\delta = \sqrt{\ln(V_\delta^2 + 1)}, \tag{27}$$

$$Q_i = \sqrt{\ln(V_{r,i}^2 + 1)}, \tag{28}$$

where $V_{r,i}$ is the total coefficient of variation for every test specimen, which is a result of the combination of the coefficient of variation of (1) the error term, and (2) the basic input variables. $V_{r,i}$ is calculated according to:

$$V_{r,i} = \sqrt{V_{r,t,i}^2 + V_\delta^2}. \tag{29}$$

The design resistance value can be calculated according to:

$$r_{d,i} = b_r * r_{t,i}(X_m) * \exp\left(-k_d * Q_i - \frac{Q_i^2}{2}\right), \tag{30}$$

for $n > 100$, and:

$$r_{d,i} = b_r * r_{t,i}(X_m) *$$
$$\exp\left(-k_d * \frac{Q_{r,t,i}^2}{Q_i} - k_{d,n} * \frac{Q_\delta^2}{Q_i} - \frac{Q_i^2}{2}\right) \tag{31}$$

for $n \leq 100$. In these equations, k_d is the design fractile factor, which is dependent on the number of test results and the reliability index β, in accordance with Annex D of EN 1990 [16]. When a reference period of 50 years and a reliability class of RC2 is assumed, the value of k_d can be assumed in accordance with Table 2.

5. For every test specimen, a safety factor can be calculated according to:

$$\gamma_{M,i}^* = \frac{r_{nom,i}}{r_{d,i}}, \tag{32}$$

where $r_{nom,i}$ is the resistance according to the design function with nominal input parameters.

The partial safety factor γ_M^* can be determined by calculating the mean of the outcomes of Eq. (32):

$$\gamma_M^* = \frac{1}{N} * \sum_{i=1}^{N} \gamma_{M,i}^*. \tag{33}$$

The evaluation of a partial safety factor, with this statistical evaluation method, will often not lead to the precise target safety factor of $\gamma_{M0} = 1.00$, due to the coupling of numerical test results and statistical data. For this reason, acceptance criteria were formulated and justified on the basis of past practice, experience, and non-exceedance

Table 3
Recommended values of f_a [14].

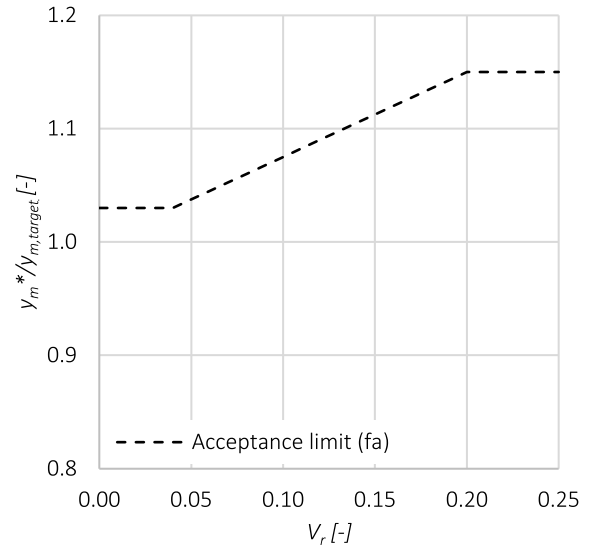| Range of V_r	Acceptance limit f_a
$0.00 < V_r < 0.04$	1.03
$0.04 \leq V_r < 0.020$	$1.03 + 0.75 * (V_r - 0.04)$
$V_r \geq 0.20$	1.15

Fig. 5. Partial factor acceptance diagram: plot of the recommended acceptance limit in relation to the coefficient of variation [14].

of probabilities. If the desired value of γ_m is termed $\gamma_{M,target}$ (in this case 1.00), the following condition can be stated:

$$\frac{\gamma_M^*}{\gamma_{M,target}} \leq f_a, \tag{34}$$

where f_a is the acceptance limit. As can be seen in Fig. 5, the values of acceptable $\gamma_M^*/\gamma_{M,target}$, are dependent on the total coefficient of variation. A low scatter may lead to probabilities of non-exceedance for the resistance values, used in the design rule, which are higher than desired. In contrast, a high scatter makes a precise choice of γ_M less relevant, in terms of failure and non-exceedance probability, even though, a high scatter is usually not desired. These observations and past practice for the selection of safety factors γ_M, were combined into a recommendation for the acceptance limit, which is shown in Table 3 and plotted in Fig. 5. If the resulting partial safety factors, calculated according to the statistical assessment procedure, do not exceed the acceptance limit, it may be concluded that the design resistance function provides an adequate reliability level if $\gamma_{M,target}$ is used [14,15].

3. FE model for the parametric study

To research the $M - V$ interaction of RHS and SHS, a 4-point bending test was modeled by means of a FE model. The non-linear FE analysis software Abaqus [22] was used to compose this model. To accurately model the difference in corner shaping of cold- and hot-formed sections, volume elements were used: firstly, shell elements were considered, nevertheless, the thickness of a hot-formed section is not uniform in the corners, making it hard to model with shell elements. A linear brick element with enhanced incompatible modes for bending (the C3D8I element) was selected from the Abaqus CEA element library [22] and employed for all models. This element type was selected as a result of an element sensitivity study involving elements with different formulations, namely C3D8, C3D8I, C3D8R, C3D20, C3D20R. Afterward, a mesh sensitivity study was performed
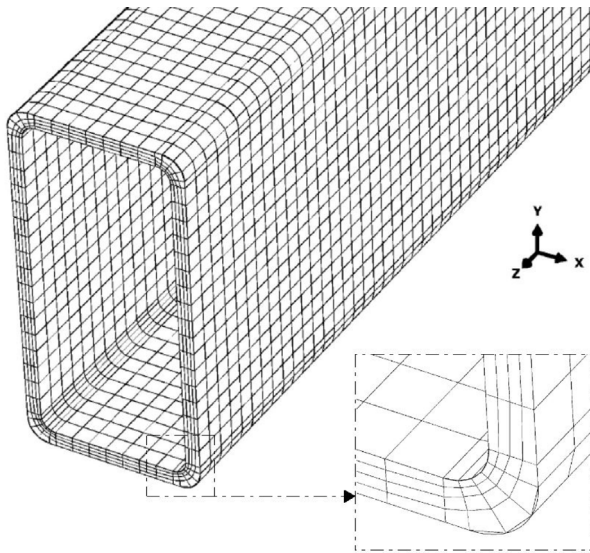
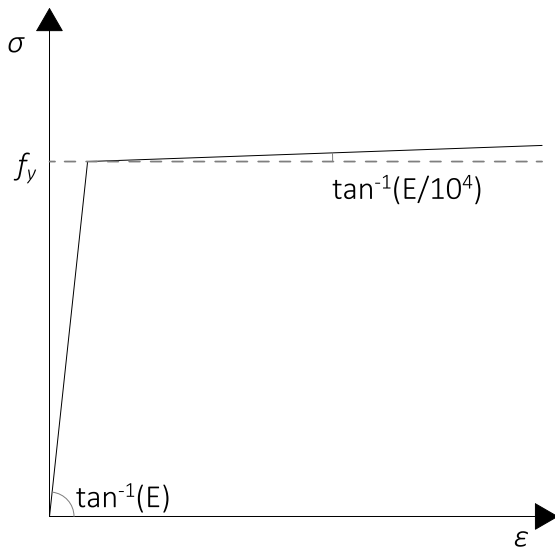**Fig. 6.** Applied mesh for FE analysis — Example of a RHS200*100/8.

Fig. 7. Stress–strain curve for bi-linear material properties in accordance with 1993-1-5, clause C.6, model b [23].

to obtain a sufficiently refined mesh, ensuring accurate and convergent stress results at practical computational costs. A mesh of four elements over the thickness and five elements over the cross-sectional corner radius of the section, with a corresponding length and width of 10 mm proved sufficient and was employed for all models. An example of this mesh configuration is shown in Fig. 6 for a hot-formed RHS200*100/8.

Bi-linear material behavior was adopted for all models, as recommended in EN1993-1-1 [1]. The stress–strain curve was calculated in accordance with EN1993-1-5 clause C.6 model b [23]. Up to the material yield strength, linear behavior was modeled. After yielding, the tangent modulus was obtained by dividing the Young modulus E by a factor of 10^4, as shown in Fig. 7.

The total span of the FE test setup was 7.5 * h and the loads were introduced at 2.5 * h, as shown in Fig. 8a. For extreme bending-dominated cases, i.e. tests with a low shear utilization ratio, an additional bending moment M_{add} was added, rotating in the same direction as the bending moment included by the applied force, as shown in Fig. 8b. For extreme shear-dominated cases, i.e. $n > 0.5$, a
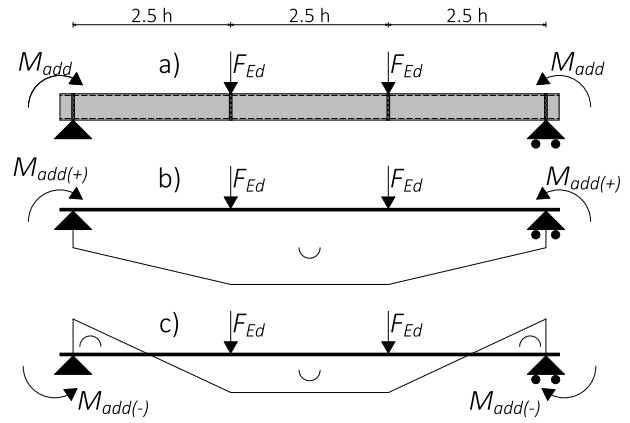

Fig. 8. (a) General test setup of the FE 4-point bending test, (b) bending moment line for bending-dominated cases, with an additional bending moment, (c) bending moment line for shear-dominated cases, with a counteracting additional bending moment.

counter-rotating additional bending moment was introduced, as shown in Fig. 8c. Both the bending moment and the applied force increased linearly up until the failure of the section. The ratio between the applied M_{add} and force F_{Ed} was different for every analysis, depending on the tested section and the required shear utilization ratio.

The boundary conditions for the supports and load introduction were implemented to match a typical experimental 4-point bending test. Fig. 9 shows the points of load introduction (L1-4) and the support points (S1 and S2) to which boundary conditions were applied. The loads were introduced at L1 and L2. In the experimental tests, performed in [11], the force was applied through stiffener plates, welded at the webs of the section. To accurately model this load introduction, L1 and L2 were constrained to a rigid body edge located at the outer side of the webs of the section. The rigid body edges made sure that the load was spread evenly throughout the section. The supports were modeled similarly at S1 and S2. The additional bending moment was introduced at L3 and L4, which were connected to the full area of the front and back surface of the section using a tie constraint.

In extreme shear-dominated cases, due to additional bending moment applied at the extremes of the beam, the bending moment at the outer sections can be higher than the bending moment in the sections adjacent to the load introduction. Since failure around the supports of the section was undesirable, the outer parts of the section, up to a length of 1.5 * h, were assigned linear material behavior. Consequently, the stress–strain relation of these parts remained linear, even after the material yield stress was reached.

The non-linear solution is obtained using the Riks algorithm [24]. Riks algorithm is generally used to obtain nonlinear static equilibrium solutions for unstable, thus allowing the determination of the failure load for a geometrically non-linear structural problem with an elastic–plastic material [25]. The goal of this FE model was to find a maximum bending moment. Since the load is introduced by mean of a force, mimicking a force-controlled test, the Riks method is needed to find post-peak decreasing loads, and thus the maximum bending resistance.

Firstly, a linear buckling analysis was performed using the Lanczos algorithm [26], resulting in different buckling shapes with corresponding eigenvalues [24]. Thereafter, a geometric and material non-linear analysis with imperfections (GMNIA) was performed, using the first positive eigenmode, with its corresponding eigenvalue, which usually corresponds to the critical buckling shape [24]. A sensitivity study was performed in which several imperfections were added to a selection of sections in two steps. Nevertheless, based on the sensitivity study, the model shows that only marginal differences in the bending resistance exist. Therefore, no imperfections are included within the FE model.
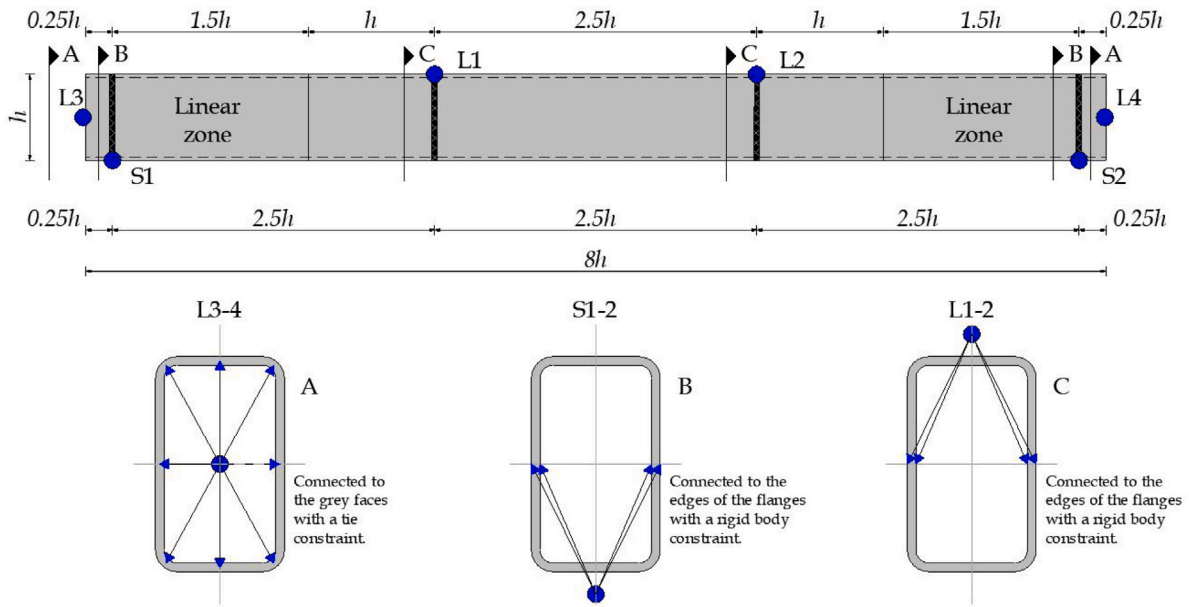
Fig. 9. Dimensions of the test setup of the FE model including a visualization of the boundary applied conditions, i.e. Loading points (L1-4), Support points (S1-2), Rigid body edges (bold black lines), and linear zones visualized in the side view and the needed cross-sections.

4. Results

The study was performed in three main phases, firstly a validation study was performed, in which an FE model was developed and compared to experimental 4-point bending tests, conducted in [11]. In this study, various element types, mesh convergences, and material properties were applied in order to test the accuracy of the model, when compared to these experimental test results. In addition, to check the convergence with respect to the mesh, the sensitivity of the ultimate load obtained with the model at a relatively high shear utilization ratio was tested. It showed that the model provides converging results if four elements over the thickness were applied, which were specifically needed for the corner regions to find convergence predicting the ultimate load. In the second phase, the validated FE model was used to conduct a parametric study, in which a selection of RHS and SHS was numerically analyzed to determine the effect of various parameters on the $M - V$ interaction of RHS and SHS, e.g. the effect of the steel grade, height over width ratio, wall thickness, and section size of the RHS and SHS. Moreover, the numerical test results were compared to the current provision of design rules regarding $M - V$ interaction of the sections, as described by Eq. (5). Lastly, new design rules were developed for the shear area and $M - V$ interaction of RHS and SHS, as explained in Section 2. These design rules were compared and fitted to the numerical test results and, after that, evaluated by means of the statistical assessment procedure [10], as described in Section 2.3.

4.1. Validation study

The developed FE model was verified with [11], mainly because of the accurate determination and documentation of material properties and imperfections of the tested RHS. Furthermore, in [11], 4-point bending tests were performed on hot- and cold-formed sections.

In [11], 44 cold-formed RHS of two different steel grades (according to Australian standards AS 1163 [27]) were tested, grade C350L0 and C450L0. In addition, two hot-formed RHS of grade S275J0H (according to European standards EN10210 [28]) were tested.

For each tested section in [11], tensile-coupon tests were performed for the middle of every corner, web, and (at least) the flange adjacent to the weld. Moreover, the height h, width b, thickness t, and outer corner radius r_e were measured for each section, as shown in Fig. 10a.
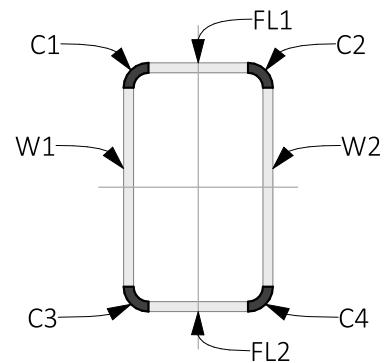
Fig. 10. (a) Basic input variables of the section and (b) the parts of the section.

The geometrical input for the FE model used these measurements. Moreover, the section was divided into eight parts, corners (C1, C2, C3, and C4), webs (W1 and W2), and flanges (FL1, FL2), as shown in Fig. 10b. To each of these parts, the material properties of the corresponding tensile-coupon test were assigned. Different from the model used in the parametric study, the material behavior is described by means of a set of monotonic true stress-true strain curves, calculated from the engineering stresses and strains, in accordance with:

$$\sigma_{true} = \sigma(1 + \epsilon),$$
$$\epsilon_{true} = \ln(1 + \epsilon). \tag{35}$$

The first study was applied to only two sections, the cold-formed RHS 150*50*4 (BF01) and the hot-formed RHS 250*150*6.3 (BH01). In both cases, the FE model underestimated the experimentally obtained maximum bending moment. For BF01 the underestimation was 10.6% and for BH01, 3.6%. Therefore, more extended research on the corner properties was performed to further optimize the configuration of the FE model. A total of six sections were selected from [11], which are shown in Table 4.

A first analysis was performed, where the material properties that resulted from the corner tensile-coupon tests, were only applied to the corners of the sections, intended as the circular trapezoid connecting each flange to the webs. However, the tensile-coupon tests were taken

Table 4
Selection of experimental tests from [11] for FE analysis.

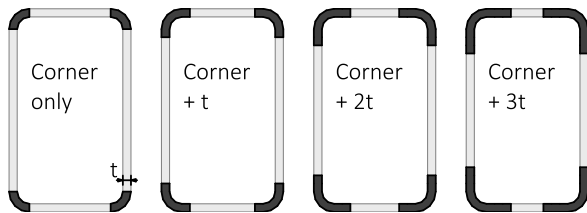| Label	h/b	Dimensions	Steel grade	HF or CF
BF01	3	150*50/4	C350	CF
BF02	3	150*50/4	C450	CF
BS06c	2	100*50/2	C450	CF
BS13c	1.67	125*75/3	C350	CF
BH01	1.67	250*150/6.3	S275	HF
BH02	1.33	200*150/6.3	S275	HF

Fig. 11. Properties of the corner tensile-coupons assigned to a part of the webs and flanges (Example CF-RHS 200*120/8 mm).

in the middle of corners, webs, and flanges. Hence, the material properties at the ends of the webs and flanges were not measured and may have shown more resemblance to the corner properties, than to the properties in the middle of the webs and flanges. Therefore, FE tests were performed on all selected sections, where the material properties of the corner were also assigned to a part of its surrounding web and flange.

Material properties of the corners were extended by t, $2t$, and $3t$, as shown in Fig. 11 for a cold-formed RHS200*120/8. Table 5 shows that, for all sections, the maximum bending moment increased when the material properties of the corners were assigned to a part of the webs and flanges. However, the increment was minimal for hot-formed sections. The difference is shown in Figs. 12 and 13. These figures show the moment–curvature diagrams of test BF01 (CF-RHS 150*50/4 mm) and test BH01 (HF-RHS 250*150*6.3 mm). Next to the experimental test data, the FE test results are shown for the sections with different corner properties. One may note that, for the cold-formed section, an increase in the area that is assigned corner properties, results in a relatively higher increase of the maximum bending moment when compared to the hot-formed section. The FE model showed the most resemblance with the experimental test results when the corner properties were extended to the webs and flanges with two times the wall thickness of the section. Henceforth, the material properties of each corner were extended to the surrounding part of the web and flange with two times the thickness of the section. With these material properties, the maximum bending moment of the FE tests was within an accuracy of 4.6% for all selected sections Table 5.

4.2. Parametric study

To assess a wide scope of cold- and hot-formed SHS and RHS, a total of 30 sections were selected for a parametric study: seventeen cold-formed sections, and thirteen hot-formed sections (Table 6). The selection is divided into three categories: small, intermediate, and large sections, with section sizes of 100, 200, and 400 mm, respectively. For every category, three different h/b ratios were tested: RHS strong axis-bending (2:1), SHS (1:1), and RHS weak-axis bending (1:2). Additionally, for cold-formed sections, the ratios (3:1) and (1:3) were selected for analysis. For hot-formed sections, these ratios are generally not fabricated. Moreover, three different section wall thicknesses t were examined for the intermediate sections: $t = 5$, $t = 8$, and $t = 12.5$ mm.

For this selection of sections, the bending resistance was numerically evaluated by means of the validated FE model. For each selected
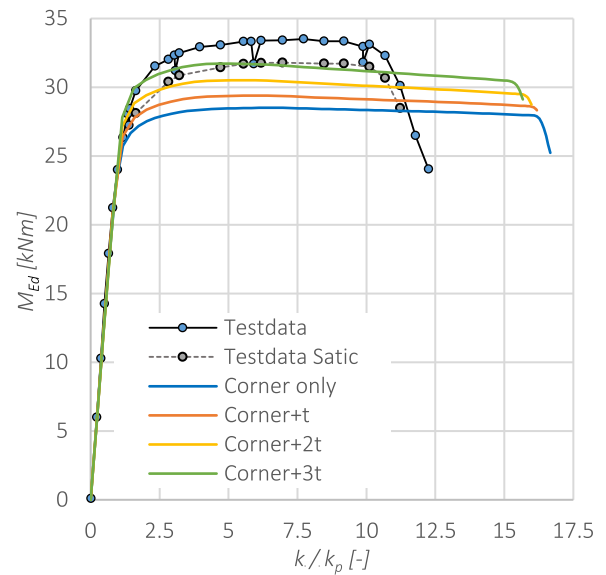
Fig. 12. Moment–curvature diagram of BF01 with different ratios of corner property extension.
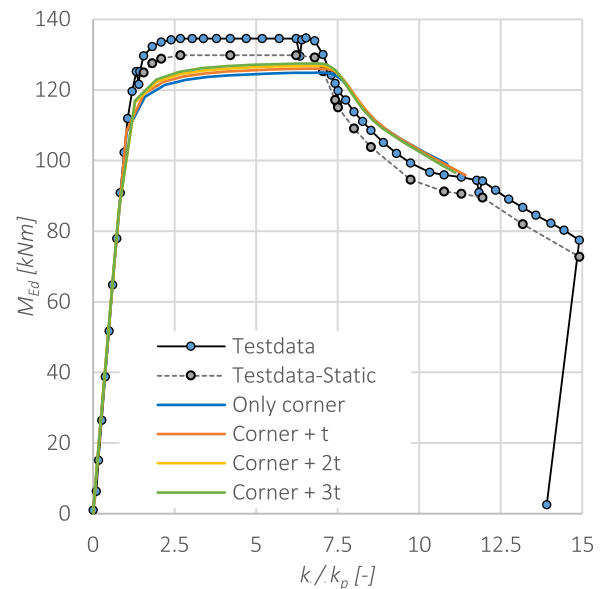
Fig. 13. Moment–curvature diagram of BH01 with different ratios of corner property extension.

section, shear utilization ratios of $n = 0.1; 0.5; 0.7; 0.8; 0.9; 1$ (if numerically possible). In some cases, shear utilization ratios higher than one was reached. For those cases, the shear utilization ratio was tested beyond the value of one until n_{max}, with varying increments depending on the tested section, where n_{max} is the maximum reached numerical shear utilization ratio.

The following effects were investigated in this parametric study.

1. Influence of the steel grade;
2. Influence of the height over width ratio;
3. Influence of the wall thickness;
4. Influence of the section size;
5. FE results compared to the current design rules.

Table 5
Absolute maximum bending moment of various FE tests and their accuracy relative to the experimental test results.

Test	Experimental	FE-Corner only		FE-Corner + t		FE-Corner + $2t$		FE-Corner + $3t$	
	[kNm]	Abs. [kNm]	Rel. [%]	Abs. [kNm]	Rel. [%]	Abs. [kNm]	Rel. [%]	Abs. [kNm]	Rel. [%]
BF01	31.9	28.5	*89.4*	29.4	*92.2*	30.5	*95.7*	31.7	*99.5*
BF02	32.0	31.3	*97.8*	32.0	*99.9*	33.0	*103.0*	34.0	*106.1*
BS06C	8.8	8.9[a]	*101.2*[a]	8.9[a]	*101.7*[a]	9.0[a]	*102.5*[a]	9.0[a]	*103.4*[a]
BS13C	19.1	19.3[a]	*100.8*[a]	19.5[a]	*101.9*[a]	19.8[a]	*103.5*[a]	20.1[a]	*105.1*[a]
BH01	129.6	124.9[a]	*96.4*[a]	126.0[a]	*97.2*[a]	126.7[a]	*97.9*[a]	127.5[a]	*98.4*[a]
BH02	96.5	100.0[a]	*103.7*[a]	100.4[a]	*104.1*[a]	100.1[a]	*104.6*[a]	101.4[a]	*105.1*[a]

[a] M_{max} reached after the curvature at the failure of the experimental test.

Table 6
Selected sections for the parametric study.

Section size	RHS [3:1] & [1:3]	RHS [2:1] & [1:2]	SHS [1:1]
Small	–	RHS 100[a]50/5	SHS 100/5
Intermediate	–	RHS 200[a]100/5	–
	RHS 300[a]100/8[a]	RHS 200[a]100/8	SHS 200/8
	RHS 300[a]100/12.5[a]	RHS 200[a]100/12.5	–
Large	–	RHS 400[a]200/12.5	SHS 400/12.5

[a]Only tested for cold-formed sections.

Table 7
Maximum shear utilization ratios n_{max} for intermediate SHS with different steel grades.

	SHS 200/5		SHS 200/8		SHS 200/12.5	
	CF	HF	CF	HF	CF	HF
S235	0.98	0.98	1.00	1.00	0.99	0.99
S355	0.99	0.96	1.00	0.98	0.98	0.96
S460	0.98	0.97	1.00	0.96	1.00	1.01

4.2.1. Influence of the steel grade

To investigate the effect of the steel grade on the $M - V$ interaction, the intermediate-sized SHS were tested for steel grade S355 and S460, in addition to steel grade S235. The results of this study are shown in Table 7. As illustrated in this table, some minor differences in the maximum shear utilization ratios may be observed. Nevertheless, the maximum difference in n_{max} between two identical sections with different steel grades is 0.05, which is very limited. Furthermore, for all selected sections and steel grades, the relative $M - V$ interaction curves look nearly identical. For example, Fig. 14 shows a comparison of the $M - V$ interaction curves of the cold-formed SHS 200/8 in steel grades S235, S335, and S460.

4.2.2. Influence of the height over width ratio

Sections with h/b ratios of 3:1, 2:1, 1:1, 1:2, and 1:3 were included for small, intermediate, and large-sized sections, to ensure that the effect of this variable on the $M - V$ interaction could be researched. The results for the selected sections are shown in Table 8, in which all values for n_{max} for the different h/b ratios are shown.

This table shows that, the numerical values of n_{max} are all within 0.05 of the theoretical maximum shear utilization ratio ($n = 1$). This minor difference is mainly caused by underestimation of the theoretical maximum shear utilization ratio for sections loaded in strong-axis bending, i.e. $h/b = 2:1$ and 3:1. The average maximum shear utilization ratio $\bar{n}$ of RHS with an h/b ratio of 3:1, equals 0.956. For a ratio of 2:1, $\bar{n} = 0.964$ for cold-formed sections, and $\bar{n} = 0.962$ for hot-formed sections.

In terms of the relative $M - V$ interaction curve, the numerical results show a clear dependency on the h/b ratio of a section, as shown in Fig. 15. Where for low shear utilization ratios, the reduction of the bending moment shows similarity for all h/b ratios, there is a large deviation of the reduction when moderate and large shear utilization ratios are reached. Sections with a relatively large shear
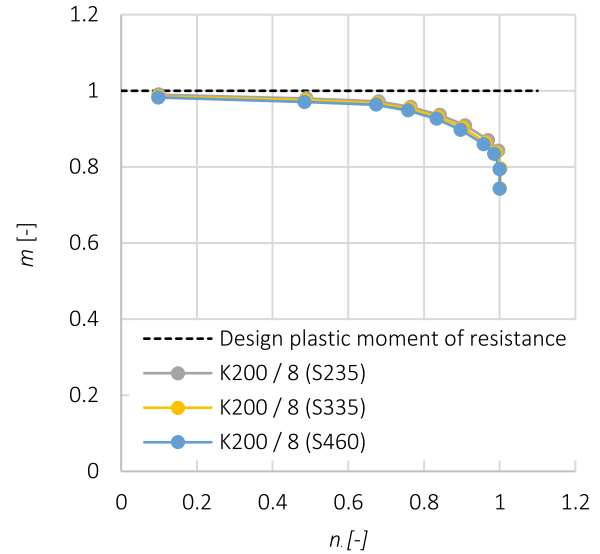

Fig. 14. Numerical relative $M - V$ interaction curves of a cold-formed SHS 200/8 with various steel grades.

Table 8
Maximum shear utilization ratios n_{max} of intermediate sections of steel grade S235 with different h/b ratios.

	Cold-formed sections				
section size	Small	Intermediate			Large
	$t = 5$	$t = 5$	$t = 8$	$t = 12.5$	$t = 12.5$
$h/b = [3 : 1]$	–	–	0.96	0.95	–
$h/b = [2 : 1]$	0.97	0.97	0.95	0.96	0.97
$h/b = [1 : 1]$	1.00	0.98	1.00	0.99	0.99
$h/b = [1 : 2]$	1.01	0.97	0.98	0.98	0.99
$h/b = [1 : 3]$	–	–	0.96	0.98	–

	Hot-Formed sections				
section size	Small	Intermediate			Large
	$t = 5$	$t = 5$	$t = 8$	$t = 12.5$	$t = 12.5$
$h/b = [2 : 1]$	0.96	0.96	0.95	0.97	0.96
$h/b = [1 : 1]$	0.99	0.99	0.99	0.98	0.98
$h/b = [1 : 2]$	0.99	0.97	0.99	0.98	0.98

area, i.e. sections loaded in strong-axis bending, generally show a larger reduction of the maximum bending moment. In contrast, sections with a low shear area (relative to the total sectional area) show relatively little reduction of the maximum bending moment.

4.2.3. Influence of the wall thickness

Three intermediate sections with different wall thicknesses were numerically tested ($t = 5$, $t = 8$, and $t = 12.5$). The resulting maximum shear utilization ratios for these sections are shown in Table 9. As
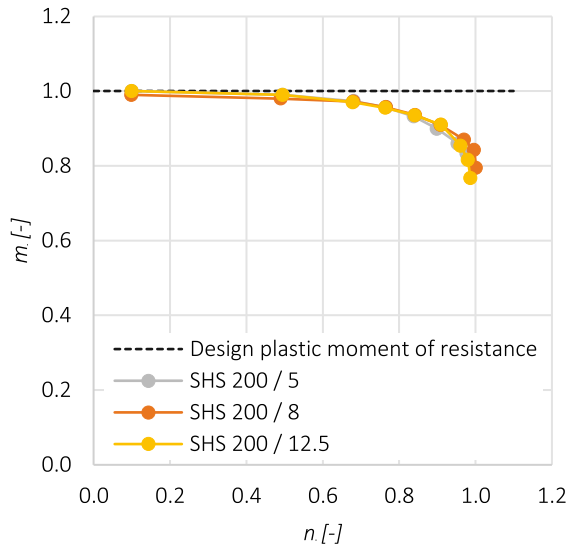
Fig. 15. Relative $M - V$ interaction curves in various h/b ratios for intermediate cold-formed sections in S235.

Table 9
Maximum shear utilization ratios n_{max} of intermediate sections in steel grade S235 with different wall thicknesses.

	Cold-formed sections				
h/b	[3:1]	[2:1]	[1:1]	[1:2]	[1:3]
$t = 5$	–	0.97	0.98	0.97	–
$t = 8$	0.96	0.95	1.00	0.98	0.96
$t = 12.5$	0.95	0.96	0.99	0.98	0.98
	Hot-formed sections				
h/b	[3:1]	[2:1]	[1:1]	[1:2]	[1:3]
$t = 5$	–	0.95	0.99	0.97	–
$t = 8$	–	0.97	0.99	0.99	–
$t = 12.5$	–	0.96	0.98	0.98	–

shown in this table, there are no clear differences between the maximum shear utilization ratios. The largest difference in the maximum shear utilization ratio for two different sections with the same h/b ratio is 0.02. This may also be noticed in the numerically obtained relative $M - V$ interaction curves, e.g. Fig. 16 shows the relative $M - V$ interaction curves for the cold-formed SHS200 with various wall thicknesses.

4.2.4. Influence of the section size

For this study regarding the effect of the section size on the relative $M - V$ interaction, small, intermediate, and large-sized sections were selected, with section sizes of 100, 200, and 400 mm, respectively. The numerical results of the small and intermediate sections with a steel grade S235 were compared for a wall thickness of 5 mm, e.g. the results of RHS 100*50/5 were compared to the results of RHS 200*100/5. Similarly, the intermediate and large sections were compared for a wall thickness of 12.5 mm.

The resulting maximum shear utilization ratios of this study are shown in Table 10. One may note that the differences of n_{max} are within 0.04 for all compared sections. For the hot-formed sections, the differences were limited to 0.01. Fig. 17 shows the numerical relative $M - V$ interaction curves of these hot-formed sections. One notes that these curves are nearly identical.

4.2.5. Numerical results compared to the current design rules

The numerical results were also compared to the current design rules in EN1993-1-1 [1]. Table 11 ($\alpha = 1$) shows a comparison of the
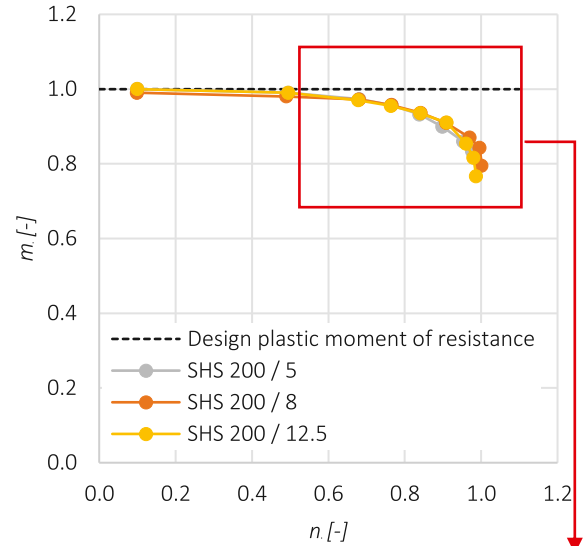

Fig. 16. Relative $M - V$ interaction curves for various thicknesses of the cold formed SHS200 in S235.

Table 10
Maximum shear utilization ratios n_{max} for different section sizes of cold- and hot-formed sections in steel grade S235.

n_{max} [1] - different section sizes - S235						
	Cold-formed sections					
	Small-Inter ($t = 5$)			Inter-Large ($t = 12.5$)		
h/b	[2:1]	[1:1]	[1:2]	[2:1]	[1:1]	[1:2]
Small	0.97	1.00	1.01	–	–	–
Intermediate	0.97	0.98	0.97	0.96	0.99	0.98
Large	–	–	–	0.97	0.99	0.99
	Hot-formed sections					
	Small-Inter ($t = 5$)			Inter-Large ($t = 12.5$)		
h/b	[2:1]	[1:1]	[1:2]	[2:1]	[1:1]	[1:2]
Small	0.96	0.99	0.99	–	–	–
Intermediate	0.96	0.99	0.97	0.97	0.98	0.98
Large	–	–	–	0.96	0.98	0.98

maximum numerical shear utilization ratio for all tested sections in S235 in percentages, where A_v is calculated in accordance with Eq. (2). The numerical results match the theoretical maximum shear utilization ratio with an accuracy of 5%. The lowest maximum shear utilization ratio of 0.95 was observed for the hot- and cold-formed RHS 200*100/8 and cold-formed RHS 300*100/12.5, tested in strong-axis bending. The highest maximum shear utilization ratio of 1.01, was obtained for the RHS 100*50/5, tested in weak-axis bending. In general, the strong-axis
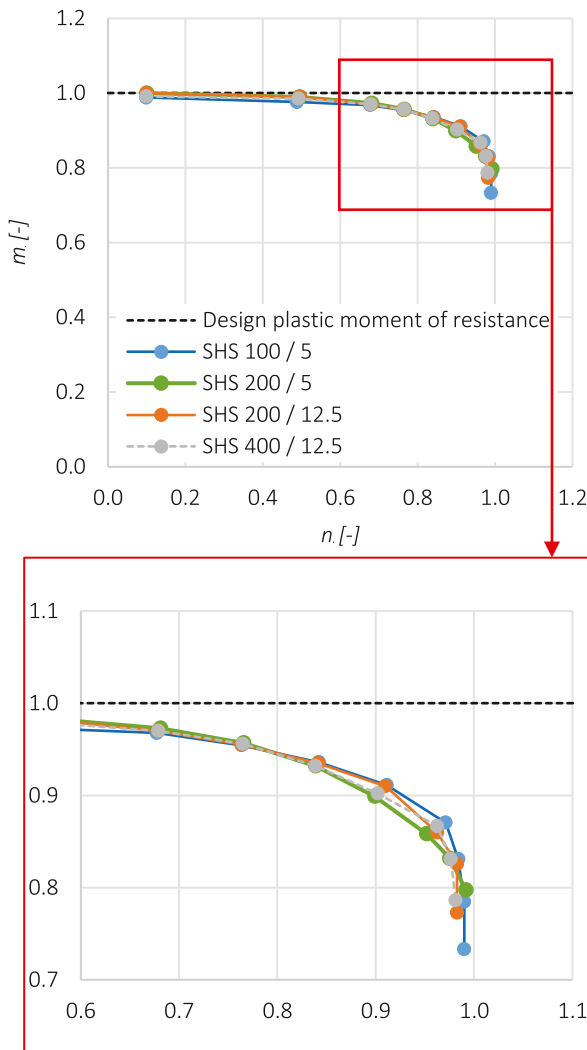
Fig. 17. Numerical relative $M-V$ interaction curves for hot-formed S235 sections with different section sizes.

bending tests showed slightly lower maximum shear utilization ratios (between 0.95 and 0.99) relative to the selected SHS sections (between 0.98 and 1.00) and RHS tested in weak-axis bending (between 0.96 and 1.01). Hence, the Eurocode 3 overestimates the numerically obtained shear utilization ratio with a maximum of 5% and the overestimation is most significant for RHS loaded in strong-axis bending.

The relative $M-V$ interaction curves of RHS and SHS are calculated according to Eq. (5), the current design rule. This equation indicates a reduction of the bending moment resistance if $n > 0.5$. To give a comparison of the theoretical $M-V$ interaction curve (according to EN1993-1-1 [1]) and the numerical $M-V$ interaction curve, both curves are plotted for a cold-formed SHS 200/8 and are shown in Fig. 18.

For cold- and hot-formed sections, the current design rule regarding $M-V$ interaction resistance, predicts reduction too late. Where for the current design rules, the reduction of the bending moment starts from $n > 0.5$, in the numerical results, a marginal reduction of the bending resistance is already observed for lower shear utilization ratios. Nevertheless, a significant reduction of the numerical bending resistance only starts from $n \approx 0.8$ for most sections. Hence, the current design rules show a too strong reduction for $n > 0.5$. For the SHS 200/8 in particular, the current design rule predicts a reduction of the bending resistance of 33,3% at $n = 1$, where the numerical results show less
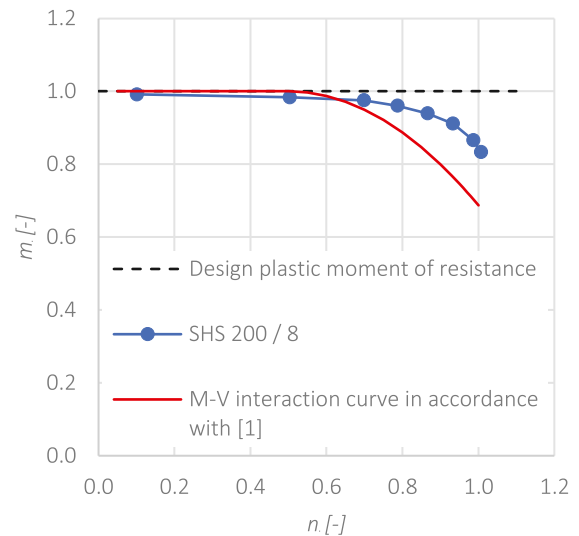

Fig. 18. Numerical relative $M-V$ resistance compared to theoretical relative $M-V$ resistance according to EN1993-1-1 [1] for a Cold-formed SHS 200/8 in S235.

reduction (around 17% at n_{max}). This difference is also observed for all other selected sections.

4.3. New design rule for the shear area

To correct for the underestimation of the shear area for sections with a larger h/b ratio, a corrected version of Eq. (2) was developed in accordance with paragraph 2.1. In the corrected version of the design rule for the shear area (Eq. (9)), an α factor was introduced and solved by means of a least square estimation. Introducing an α factor in front of the variable h/b in the denominator accounts for larger corrections for large, and minimal corrections for small h/b ratios.

The least square estimation was performed according to the explained procedure in Section 2.1. The numerical data of the maximum shear utilization ratio of all tested sections of steel grade S235 were taken into account in this estimation, which was solved for the optimal value of α. The least square residuals were found for $\alpha \approx 1.05$, with a corresponding R^2 value of 0.99982. Table 11 shows the comparison of the numerically obtained shear area with the theoretical shear area, and adjusted design rule in accordance to Eq. (9) with $\alpha = 1.05$, for all 34 sections of steel grade S235. Fig. 19 visualizes the difference in shear area between the current and new design rule, for a cold-formed RHS 200*120/8. The new design rule results in a slightly lower shear area for all sections. The mean shear area is approximately 100% for the new design rule, as shown in Table 11, whereas the current design rule overestimates the shear area with 2.4% on average. Moreover, the new design rule for the shear area describes the FE test results within an accuracy of a maximum of 2.9%. The maximum overestimation of the numerically obtained shear area, according to the current design rule, is 5.1%. Hence, the new design rule for the shear area results in a more balanced and accurate prediction of the numerically obtained shear area, when compared to the current design rule used in EN1993-1-1 [1].

4.4. New design rule for $M-V$ interaction

Apart from a new design rule for the shear area, a new design rule for the $M-V$ interaction of RHS and SHS is proposed in Section 2.2. Fig. 20 shows the relative $M-V$ interaction curves for hot-formed RHS 200*100/5, tested in (a) strong- and (b) weak-axis bending, together with the theoretical $M-V$ interaction curves, based on the Tresca and Von Mises yield criterion as in Eqs. (3) and (6). The graphs in this

Table 11
Numerically obtained shear area of all S235 sections compared to the shear area calculated according to the current ($\alpha = 1$) and new ($\alpha = 1.05$) design rule.

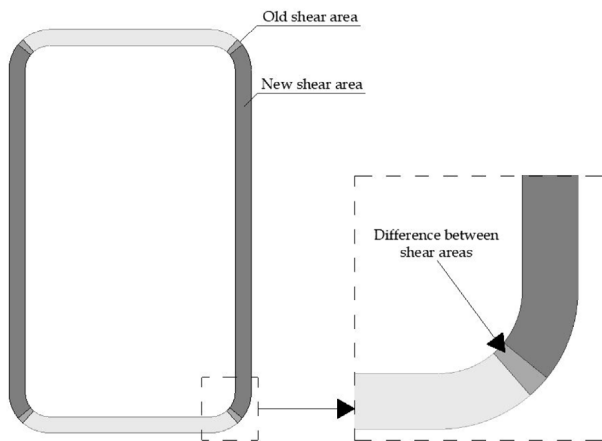| Section information				Design rules based shear area			
Section	HF/CF	Axis	$A_{v,FEA}$	Current ($\alpha = 1$)		New ($\alpha = 1.05$)	
			[mm²]	A_v [mm²]	$A_v/A_{v,FEA}$ [%]	$A_{v,new}$ [mm²]	$A_{v,new}/A_{v,FEA}$ [%]
RHS 100*50/5	CF	Strong-axis	862	891	103.4	862	100.0
RHS 200*100/5	CF	Strong-axis	1829	1891	103.3	1830	100.0
RHS 200*100/8	CF	Strong-axis	2742	2883	105.1	2790	101.7
RHS 200*100/12.5	CF	Strong-axis	3977	4136	104.0	4003	100.7
RHS 300*100/8	CF	Strong-axis	4265	4443	104.2	4282	100.4
RHS 300*100/12.5	CF	Strong-axis	6212	6528	105.1	6292	101.3
RHS 400*200/12.5	CF	Strong-axis	8881	9136	102.9	8841	99.6
SHS 100/5	CF	–	920	918	99.7	896	97.3
SHS 200/5	CF	–	1874	1918	102.3	1871	99.8
SHS 200/8	CF	–	2967	2962	99.8	2890	97.4
SHS 200/12.5	CF	–	4297	4352	101.3	4246	98.8
SHS 400/12.5	CF	–	9212	9352	101.5	9124	99.0
RHS 100*50/5	CF	Weak-axis	449	445	99.1	438	97.5
RHS 200*100/5	CF	Weak-axis	917	945	103.1	930	101.4
RHS 200*100/8	CF	Weak-axis	1414	1441	101.9	1418	100.3
RHS 200*100/12.5	CF	Weak-axis	2029	2068	101.9	2034	100.3
RHS 300*100/8	CF	Weak-axis	1421	1481	104.2	1463	102.9
RHS 300*100/12.5	CF	Weak-axis	2136	2176	101.9	2149	100.6
RHS 400*200/12.5	CF	Weak-axis	4511	4568	101.3	4493	99.6
RHS 100*50/5	HF	Strong-axis	119	915	103.9	886	100.6
RHS 200*100/5	HF	Strong-axis	249	1915	104.4	1854	101.0
RHS 200*100/8	HF	Strong-axis	386	2983	104.9	2887	101.5
RHS 200*100/12.5	HF	Strong-axis	591	4471	102.6	4327	99.3
RHS 400*200/12.5	HF	Strong-axis	1236	9471	103.9	9166	100.6
SHS 100/5	HF	–	126	937	101.0	914	98.5
SHS 200/5	HF	–	261	1937	100.8	1889	98.4
SHS 200/8	HF	–	405	3038	101.8	2963	99.3
SHS 200/12.5	HF	–	614	4604	101.8	4491	99.3
SHS 400/12.5	HF	–	1279	9604	101.9	9369	99.4
RHS 100*50/5	HF	Weak-axis	61	458	101.4	450	99.7
RHS 200*100/5	HF	Weak-axis	127	958	102.6	942	100.9
RHS 200*100/8	HF	Weak-axis	201	1492	100.8	1467	99.1
RHS 200*100/12.5	HF	Weak-axis	297	2236	102.0	2199	100.3
RHS 400*200/12.5	HF	Weak-axis	630	4736	102.0	4658	100.3
Maximum					105.1		102.9
Minimum					99.1		97.3
Mean					102.4		99.9

Fig. 19. Old and new shear area of a cold-formed RHS 200*120/8.

figure show that, where Eq. (3) predicts no reduction for low shear utilization ratios, Eq. (6) predicts too excessive reduction, relative to the numerically obtained relative $M - V$ interaction curve. Nevertheless, the $M - V$ interaction curve, according to the Von Mises yield criterion, shows more resemblance with the numerically obtained relative $M - V$ interaction curve than the current design rule.

An adapted version of the Von Mises yield criterion with a higher order root was developed (Eq. (14)) to compensate the current design rule for (1) the uniform reduction of the strength for the total shear area, and (2) the direct stresses that may arise in the shear area, as described in 2.2. To find the optimal value of P in Eq. (14), a least square estimation was performed [17]. All 34 sections were taken into account for this estimation, each with a number of data points as a result of the various tested shear utilization ratios (varying from $N = 6$ up to and including $N = 10$). P was solved for the minimal summation of the squared residuals, which resulted in $P = 5.443$ and a corresponding R^2 value of 0.84.

The design rule was plotted with the optimal value of P for hot-formed RHS 200*100/5, tested in (a) strong- and (b) weak-axis bending, which is shown in Fig. 20. The relative $M - V$ interaction curve, based on the new design rule, shows a significantly better fit to the numerical data than the current design rule in EN1993-1-1 [1]. Generally, the new design rule gives a fairly accurate estimation of the numerically obtained $M - V$ resistance for low and moderate shear utilization ratios. Nevertheless, the $M - V$ resistance of sections, subject to an extremely high shear utilization ratio ($n > 0.95$), is hard to predict, since the numerical reduction deviates substantially for different sections.

4.5. Validation of new design rule for the shear area

The newly developed design rules are validated by means of the statistical assessment procedure described in paragraph 2.3. In the evaluation of the shear area, 34 sections were included ($N = 34$). The
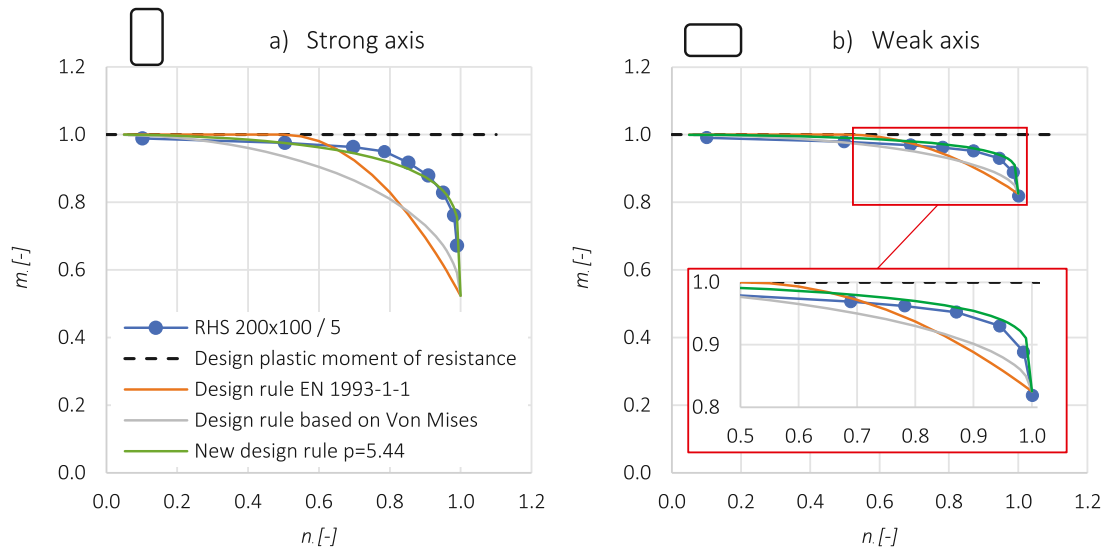
Fig. 20. Numerical relative $M - V$ resistance of RHS 200*100/5 results in (a) strong-axis bending and (b) weak axis-bending compared to various theoretical $M - V$ resistance functions and the newly developed design rule.

numerically obtained shear resistance served as r_{exp} and the theoretical shear resistance as r_t, which was calculated according to Eq. (13) with $\alpha = 1.05$ in Eq. (9).

For every section, various parameters were established. Firstly, the mean value of correction factor b_r was calculated, which resulted in $b_r = 1.0017$. This value is close to one, which indicates that there is little difference between the numerical and the theoretical resistance. Secondly, the coefficient of variation of the error term and the basic input variables were calculated. This resulted in $V_\delta = 0.0126$ and a unique coefficient of variation of the basic input variables for every section. the partial derivatives of the resistance design function were derived numerically, according to Eq. (25).

With this information, a total coefficient of variation V_r and a design resistance value r_d were calculated for each section. Since $N \leq 100$, Eq. (31) was used to calculate the design resistance. For this calculation, the value of $k_{d,n} = 3.14$ is used. A partial safety factor was calculated for each section. The mean value of all partial safety factors was calculated, which resulted in $\gamma_M^* = 0.837$ with a coefficient of variation of 0.000796.

The acceptance limit was plotted for all sections (Fig. 21). In this figure, the scatter is barely noticeable, since the differences in V_r and γ_m^* are extremely small for all sections. Nevertheless, the obtained safety factor is far below the acceptance limit for all sections. Hence, an adequate reliability level is obtained if $\gamma_{M0} = 1.0$ is used for all tested sections.

4.6. Validation of new design rule for $M - V$ interaction

In addition to the validation of the new design rule for the shear area, the new design rule for the $M - V$ interaction of RHS and SHS was validated (Eq. (15)). This equation contains the variables M_{pl} and W_{pl}, which are based on the basic input variables of the section (h, b, t, r_e, r_i, and f_y). To calculate the coefficient of variation of the basic input variables, Eq. (15) was rewritten as a function of these variables. This was carried out by calculating the plastic bending moment, with W_{pl} according to:

$$W_{pl} = \sum_{i=1}^{S} A_{v}, i * y_i, \tag{36}$$

where A_i is a partial area of the total sectional area and y_i is the corresponding distance of the y-coordinate of the center of gravity of A_i to the center of gravity of the section. The plastic section modulus
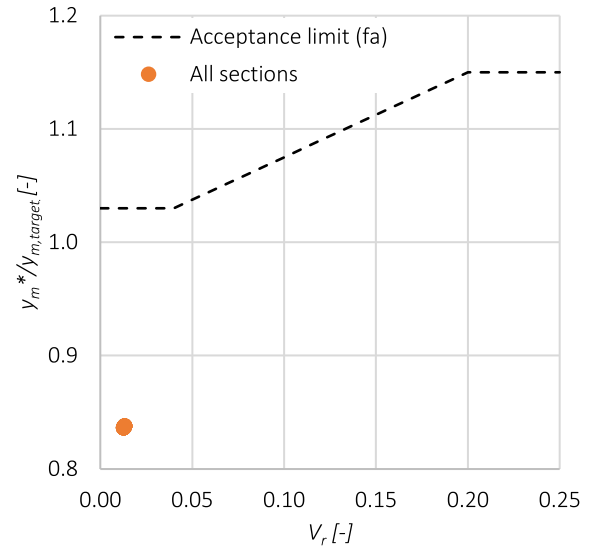

Fig. 21. Acceptance diagram for the design rule for the shear resistance.

of the shear area only $W_{pl,v}$, can be calculated by only taking the shear area in Eq. (36) and multiplying it with its corresponding y_i. In case of an RHS or SHS, the total area A can be subdivided in three different areas, the area of the flanges A_{fl}, webs A_w, and corners A_c, calculated according to (37), (38), and (39), respectively, and shown in Fig. 22.

$$A_{fl,CF} = (b - 2r_e) * 2t,$$
$$A_{fl,HF} = (b - 4t) * 2t, \tag{37}$$

$$A_{w,CF} = (h - 2r_e) * 2t,$$
$$A_{w,HF} = (h - 4t) * 2t, \tag{38}$$

$$A_{c,CF} = \pi * (r_e^2 - r_i^2),$$
$$A_{c,HF} = 4 * ((2t)^2 - \frac{\pi * t^2}{4} - (r_e^2 - \frac{\pi * r_e^2}{4})). \tag{39}$$

The plastic section modulus of the shear area was calculated according to:

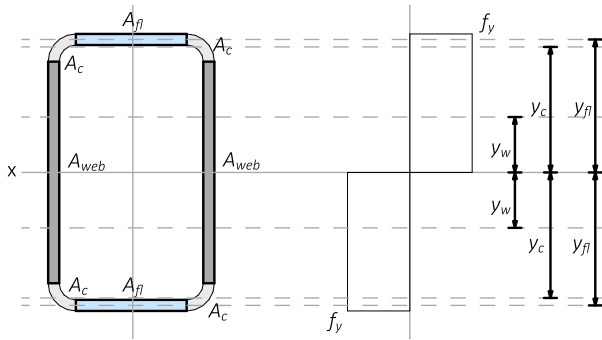$$W_{pl,v} = A_{v,new} * y_v, \tag{40}$$

Fig. 22. Different areas of an RHS section and the distances of these areas to the center of gravity of the RHS.

where $y_v = (h - 2t)/4$ and $A_{v,new}$ is calculated according to Eq. (9). This is a simplified calculation where the center of gravity is calculated with the shear area treated as a rectangle, where, in reality, the part of the corners, which is a part of the shear area of the section, might give a slightly different value of y_v. The new design rule for the shear area was used in this statistical evaluation.

Using this definition of the $M - V$ resistance, $r_{exp,i}$ and r_{t_i} were calculated according to Eq. (41) and (42), respectively:

$$r_{exp,i} = M_{Rd,FEM,i}, \qquad (41)$$

$$r_{t,i} = M_{pl} - W_{pl,v} * (f_y - f_{y,r,new}), \qquad (42)$$

where, $M_{Rd,FEM,i}$ is the maximum bending moment as a result of the FE simulations for every specimen.

In total, 34 sections were tested numerically for various shear utilization ratios. For every included section, different shear utilization ratios were used (varying from 6 up to and including 9). Altogether, a total of 261 data points ($N = 261$) were taken into account for this statistical evaluation.

The b_r value was calculated for every section, together with the total coefficient of variation (based on V_δ and $V_{r,t}$). The partial derivatives of the resistance function were calculated by means of a numerical estimation, according to Eq. (25). Hereafter, the value of resistance r_d was calculated. Since the statistical analysis was performed for every section separately, r_d was calculated according to Eq. (31) with $k_{d,\infty} = 3.04$ and $k_{d,n}$ depending on the number of shear utilization ratios for section i as a subset of all sections. Lastly, a mean partial safety factor was calculated for every section.

The obtained partial safety factor was below the acceptance limit for all sections, which indicates good performance of the resistance design function. Fig. 23 shows a plot of the acceptance diagram, in which the mean partial safety factors were plotted for each section, together with the acceptance limit (in accordance with Table 3). The overall mean value of the safety factors resulted in $\gamma_M^* = 0.979$. Hence, an adequate reliability level is obtained if $\gamma_{M0} = 1.0$ is used for all tested sections.

5. Discussion

Validation and parametric study

The validation of the FE model is based on test data in [11]. The final FE model is able to predict the experimental maximum bending moment with an accuracy of 5%. Most likely, the main cause of the remaining inaccuracy is the lack of material data in the experimental tests [11]. Tensile coupon tests were only taken in the corners and center of the webs and flanges and the imperfections of the sections were not measured to full extent. For the parametric study, bi-linear stress–strain curves and nominal section dimensions were used. In the parametric study, for all tests with low shear utilization ratios,

the difference between the numerical bending resistance and M_{pl} was negligible. Hence, it is expected that the inaccuracy of the results of the validation study is largely caused by a lack of material input data.

The parametric study was performed making use of the validated FE model. The size, wall thickness, and steel grade of the section do not seem to affect the maximum shear utilization ratio and relative $M - V$ interaction resistance of RHS and SHS. Nevertheless, sections with a larger shear area (relative to the total sectional area) show a larger reduction of the bending resistance with an increase in the shear utilization ratio. This dependency was expected and is taken into account in the current design rules for $M - V$ interaction, prescribed by EN1993-1-1 [1].

Comparison of the FE-results and the current design rules

When a comparison is made between the FE results and the current design rules for $M - V$ interaction, various discrepancies were observed. Firstly, the current design rule in EN1993-1-1 [1] only initiates a reduction of the bending resistance for $n > 0.5$, whereas the FE results also show a marginal reduction of the bending resistance for lower shear utilization ratios for all tested sections. Furthermore, for $n > 0.5$, the current $M - V$ interaction design rules in EN1993-1-1 [1] prescribe a conservative bending resistance i.e. too much reduction of the bending resistance. The numerical bending resistance is generally higher than the currently prescribed bending resistance for $n > 0.5$. This problem is more significant for the larger h/b ratios.

Two explanations may be provided for the discrepancies between the FE results and the current design rules. Firstly, the current design rules prescribe a reduction of the bending resistance based on a uniform distribution of the shear stresses within the shear area, whereas in practice, the shear stresses are not uniformly distributed over the shear area. By theory, the maximum shear stresses are located in the middle of the shear area and the shear stresses decrease toward the outer fibers of the section. Hence, a uniform reduction of the direct stresses in the shear area provides a conservative approximation of the bending resistance. Secondly, the current design rule for $M - V$ interaction is based on 2D beam theory, where in reality, complex elastic–plastic 3D stress states occur in the section. Although, in accordance with the current design rule, direct stresses are not predicted in the shear area when $n = 1.0$, in the numerical results, direct stresses in the outer fibers of the section were observed for the maximum shear utilization ratio analyses. Hence, due to these direct stresses, the actual bending resistance of RHS and SHS may be higher than the theoretical bending resistance.

When a similar comparison is made for the shear area, the numerical results show a close resemblance with the current design rules. The current design rule for the shear area describes the numerically obtained shear area with an accuracy of 5% or better, for all sections. However, it overestimates the numerically obtained shear area with 2.4% on average. Larger overestimations are observed for RHS, tested in strong-axis bending, i.e. $h/b = 2:1$ and $3:1$. Therefore, a new design rule was developed.

Development and assessment of design rules

The current design rule for the shear area was slightly modified for the overestimation of the larger h/b ratios by means of a correction factor $\alpha = 1.05$ in the denominator of the current design rule. Putting this correction factor only in front of variable h or b (depending on the direction of loading), results in a larger compensation of the shear area for larger h/b ratios, which is desirable. The optimal value of $\alpha = 1.05$ was found by a least square estimation. The new design rule for the shear area described the numerically obtained shear area with an accuracy of a maximum of 2.9% and with an underestimation of 0.1% on average.

The new design rule for the shear area was evaluated by means of a statistical assessment procedure [10,14,15]. which resulted in $\gamma_M^* = 0.837$. This partial safety factor is relatively low. The reason for this
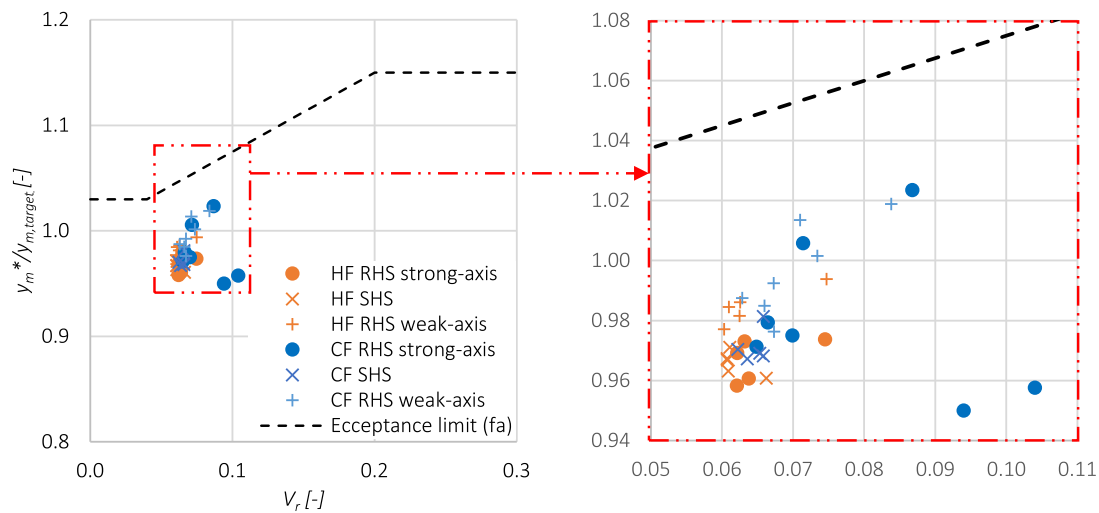
Fig. 23. Acceptance diagram for the design rule based on the Von Mises yield criterion.

is the accuracy of the resistance function. Since there is very little difference between the numerical and theoretical shear resistance, the total coefficient of variation is fairly low and the mean value of the correction factor b_r is close to one. In Eq. (31), b_r is multiplied by the resistance function with the mean/nominal values of the basic input parameters, in accordance with Table 1. The last part of this function represents the reduction of the design resistance as a result of the coefficient of variation. One may notice that if V_r approximates zero, the value within the exponent of this function approximates 0 as well, which results in $exp(0) = 1$. Hence, if there is an extremely low scatter and coefficient of variation, the partial safety factor will approach $r_{d,i} \approx r_{t,i}(X_m)$. here, $r_{t,i}/r_{t,i}(X_m) \approx 0.8$ for all sections, since the mean value of the yield strength is taken into account in the evaluation. For S235 the mean yield strength is $1.25 * f_y$, where f_y is the nominal yield strength and $1.25/1 = 0.8$. Therefore, a partial safety factor of 0.837 indicates a low scatter and an accurate resistance design function, i.e. in this case, the newly developed design rule for the shear resistance.

Because of this low partial safety factor, one may criticize the practical use of the compensation of the shear area. The current design rules give a slight overestimation of the shear area for the large h/b ratios. Nevertheless, the current design rule for the shear area will most likely still result in a partial safety factor well below $\gamma_M^* = 1.0$. Hence, even though the current design rule for the shear area is not completely accurate, it still gives a presentable and safe prediction of the shear resistance.

For the $M-V$ interaction, a design rule was developed based on a higher order root function of the Von Mises yield criterion. The $M-V$ interaction curve, according to the Von Mises yield criterion, already results in a reduction of the bending resistance for $n > 0$. Nevertheless, like the current design rule for $M-V$ interaction resistance, this design rule also results in a conservative reduction of the bending resistance, most likely due to the same reasons as explained in the previous paragraph. To adjust for this reduction, a least square fit was made for a higher order degree P in the original Von Mises $M-V$ interaction resistance design rule. This resulted in a decent prediction of the numerical $M-V$ interaction resistance, with a value of $P = 5.44$.

Nevertheless, it is hard to predict the reduction of the bending resistance for extremely high shear utilization ratios, since the numerical reduction deviates substantially for different sections for shear utilization ratios of $n \geq 0.95$. In some cases, for RHS loaded in weak-axis bending, the new design rule resulted in a slightly unsafe approximation of the bending resistance in some cases. This could be the result of a limited amount of FE simulations. When more shear utilization ratios are simulated numerically, the deviation in reduction

of the maximum bending moment might decrease. On the other hand, in practice, these extreme shear utilization ratios are unrealistic.

Lastly, the newly developed design rule was evaluated by means of a statistical assessment procedure [10,14,15]. A mean partial safety factor of $\gamma_M^* < 1$ was obtained. Hence, an adequate reliability level is obtained if $\gamma_{M0} = 1.0$ is used for all tested RHS and SHS.

6. Conclusions

It is concluded that the size, wall thickness, and steel grade of a section have little to no effect on the relative shear and $M-V$ resistance of RHS and SHS. Nevertheless, the height/width ratio of the section has a significant effect on the relative $M-V$ interaction curve of RHS and SHS. Sections with a larger shear area (relative to the total sectional area) show a larger reduction of the bending resistance together with an increase in the shear utilization ratio.

The current design rule for the shear area is relatively accurate (within 5%), but overestimates the numerically obtained shear area with an average of 4.4%. The larger overestimations were observed for $h/b = 2:1$ and 3:1. Hence, a more balanced and accurate design rule for the shear area was developed.

Secondly, the current design rule for $M-V$ resistance reduces the bending resistance too late. A minor reduction of the numerically obtained bending resistance is already observed for $n > 0$, where the current design rule only states reduction for $n > 0.5$. However, once reduction is initiated, too much reduction of the bending resistance is prescribed. Thus, in addition to a new design rule for the shear area, a new design rule for the $M-V$ interaction resistance, which describes the numerical $M-V$ interaction resistance more accurately, was developed.

The newly developed design rule for the shear area accurately describes the numerically obtained shear area for all tested sections and, generally, gives a better prediction of the shear area than the current design rule in EN1993-1-1 [1]. The new design rule describes the shear area of RHS and SHS with a maximum deviation of 2.9%. Furthermore, an adequate reliability level is obtained if $\gamma_{M0} = 1.0$ is used for the application of this design rule. Nonetheless, the difference between the current and new design rule is only marginal and the current design rule also gives a safe approximation of the shear area, even though it is slightly less accurate.

The new design rule, which was developed for the $M-V$ interaction of RHS and SHS, gives a more accurate prediction of the $M-V$ interaction resistance than the current design rule. Moreover, an adequate reliability level is obtained if $\gamma_{M0} = 1.0$ is used. Nevertheless, it is hard to predict the reduction of the bending resistance for extremely high

shear utilization ratios, since the numerical reduction then deviates strongly for different sections.

This design rule, in accordance with Eq. (15), is based on the Von Mises yield criterion with an adapted higher-order root. A limitation of this design rule is that, for RHS tested in weak-axis bending, it could result in a slightly unsafe approximation, which is not desirable. Nevertheless, this overestimation is marginal and only occurs for shear utilization ratios of $n > 0.8$, which are uncommon in practice. With this knowledge, in combination with the shown adequate reliability level for $\gamma_{M0} = 1.0$, it may be concluded that the newly developed design rule gives a safe approximation of the $M - V$ interaction of RHS, which is less conservative than the current design rule, especially for shear utilization ratios $n > 0.5$.

Summarized, the current design rule for the shear area, prescribed in EN1993-1-1 [1] is relatively accurate, but overestimates the numerically obtained shear area marginally. Secondly, the current $M - V$ interaction design rule reduces the bending resistance for the presence of shear force (1) too late (at $n > 0.5$), and (2) too strongly after reduction is initiated (for $n > 0.5$). The newly developed design rules provide a more accurate prediction of the shear area, shear resistance, and $M - V$ interaction curve of RHS and SHS, compared to the design rules in EN1993-1-1 [1]. Moreover, for both newly developed design rules, it was shown that an adequate reliability level is obtained if a unit partial safety factor is used.

CRediT authorship contribution statement

Thomas Haan: Methodology, Formal analysis, Writing – original draft. **Davide Leonetti:** Conceptualization, Supervision, Review & editing. **Herm Hofmeyer:** Supervision, Review & editing. **H.H (Bert) Snijder:** Conceptualization, Supervision, Review & editing.

Declaration of competing interest

The authors declare that they have no known competing financial interests or personal relationships that could have appeared to influence the work reported in this paper.

Data availability

Data will be made available on request.

References

[1] CEN, EN 1993-1-1: Eurocode 3: Design of Steel Structures. Part 1-1: General rules and rules for buildings, European Committee for Standardization, 2005.

[2] D.C. Drucker, The Effect of Shear on the Plastic Bending of Beams, American Society of Mechanical Engineers, 1956.

[3] A. Carpinteri, Structural Mechanics: A Unified Approach, CRC Press, 2017.

[4] M.R. Horne, The plastic theory of bending of mild steel beams with particular reference to the effect of shear forces, Proc. R. Soc. A 207 (1089) (1951) 216–228.

[5] J. Heyman, V. Dutton, Plastic design of plate girders with unstiffened webs, Weld. Met. Fabr. 22 (1954) 265–272.

[6] A. Green, A theory of the plastic yielding due to bending of cantilevers and beams. Part ii., J. Mech. Phys. Solids 3 (2) (1955) 143–155.

[7] B.G. Neal, The effect of shear and normal forces on the fully plastic moment of a beam of rectangular cross section, J. Appl. Mech. 28 (2) (1961) 269–274, http://dx.doi.org/10.1115/1.3641666.

[8] B.G. Neal, Effect of shear force on the fully plastic moment of an I-beam, J. Mech. Eng. Sci. 3 (3) (1961) 258–266.

[9] R.W.A. Dekker, Bending Moment-Shear Force Interaction of Rolled I-Shaped Steel Sections (Ph.D. dissertation), Eindhoven University of Technology, 2019.

[10] L.S. da Silva, T. Tankova, L. Marques, U. Kuhlmann, A. Kleiner, J. Spiegler, H.H. Snijder, R.W.A. Dekker, A. Taras, N. Popa, Standardization of safety assessment procedures across brittle to ductile failure modes, Eur. Comm. Res. Fund Coal Steel (2017).

[11] T.J. Wilkinson, The Plastic Behaviour of Cold-Formed Rectangular Hollow Sections (Ph.D. dissertation), University of Sydney. Department of Civil Engineering, 1999.

[12] L. Gardner, N. Saari, F. Wang, Comparative experimental study of hot-rolled and cold-formed rectangular hollow sections, Thin-Walled Struct. 48 (7) (2010) 495–507.

[13] J. Wang, S. Afshan, M. Gkantou, M. Theofanous, C. Baniotopoulos, L. Gardner, Flexural behaviour of hot-finished high strength steel square and rectangular hollow sections, J. Construct. Steel Res. 121 (2016) 97–109.

[14] A. Taras, V. Dehan, L. da Silva, L. Marques, T. Tankova, Guideline for the Safety Assessment of Design Rules for Steel Structures in Line with EN 1990, Deliverable D1. 1, Tech. rep, SAFEBRICTILE RFSR-CT-2013-00023, 2016.

[15] A. Taras, L. Simoes da Silva, L. Marques, U. Kuhlmann, H. Snijder, Harmonization of the safety level of design rules for steel structures–from ductile to brittle failure modes, in: Proceedings of the 7th European Conference on Steel and Composite Structures, University of Naples-Federico II, Eurosteel, 2014.

[16] CEN, EN 1990: Eurocode 0 — Basis of structural design, European Committee for Standardization, 2002.

[17] S.J. Miller, The method of least squares, Math. Dep. Brown Univ. 8 (2006) 1–7.

[18] N.J. Nagelkerke, et al., A note on a general definition of the coefficient of determination, Biometrika 78 (3) (1991) 691–692.

[19] H. Abdi, et al., The method of least squares, Encycl. Meas. Stat. 1 (2007) 530–532.

[20] O. Bauchau, J. Craig, Euler-Bernoulli beam theory, in: Structural Analysis, 2009, pp. 173–221,

[21] CEN, PrEN 1993-1-1: Eurocode 3: Design of Steel Structures. Annex E: Basis for the Calibration of Partial Factors, European Committee for Standardization.

[22] Dassault Systémes, Abaqus/CEA (6.19), 2017, [Computer software].

[23] B. Johansson, R. Maquoi, G. Sedlacek, C. Müller, D. Beg, et al., "Commentary and worked examples to EN 1993-1-5" plated structural elements, JRC Sci. Tech. Rep. (2007).

[24] L.S. da Silva, T. Tankova, L. Marques, U. Kuhlmann, A. Kleiner, J. Spiegler, H.H. Snijder, R. Dekker, A. Taras, N. Popa, 13.02: Safety assessment across modes driven by plasticity, stability and fracture, Ce/papers 1 (2–3) (2017) 3689–3698.

[25] M. Zhao, On nonlinear buckling and collapse analysis using riks method, in: Abaqus Users' Conference, Simulia, 2008, pp. 1–9.

[26] S. Peng-Li, Buckling analysis of nonlinear structures using lanczos method, Comput. struct. 36 (6) (1990) 1111–1120.

[27] AS1163:1991A, Cold-Formed Structural Steel Hollow Sections, Standards Australia, 1991.

[28] EN-10210, Hot Finished Structural Hollow Sections of Non-Allow and Fine Grain Structural Steels: Part 1 - Technical Delivery, European committee for Standardization, 1994.